T-cell dysregulation and inflammatory process in Gcn2 (Eif2ak4 −/−) deficient rats in basal and stress conditions

Juliette Bignard, Fabrice Atassi, Olivier Claude, Maria-Rosa Ghigna, Nathalie Mougenot, Bahgat Soilih Abdoulkarim, Florence Deknuydt, Aurélie Gestin, Virginie Monceau, David Montani, et al.

T-cell dysregulation and inflammatory process in Gcn2 (*Eif2ak4*$^{-/-}$) deficient rats in basal and stress conditions

Juliette Bignard[1], Fabrice Atassi[1], Olivier Claude[1], Maria-Rosa Ghigna[2,3], Nathalie Mougenot[4], Bahgat Soilih Abdoulkarim[3], Florence Deknuydt[5], Aurélie Gestin[5], Virginie Monceau[1#], David Montani[3,6], Sophie Nadaud[1*], Florent Soubrier[1*], Frédéric Perros[3,7*]

1. UMR_S 1166, Sorbonne Université ; INSERM, F-75013 Paris, France

2. Department of Pathology, Institut Gustave Roussy, Villejuif

3. UMR_S999 Université Paris–Saclay, INSERM. Hôpital Marie Lannelongue, Le Plessis Robinson.

4. Sorbonne Université, UMS28, Plateforme d'Expérimentation Cœur, Muscles, Vaisseaux (PECMV), 75013, Paris, France

5. Flow cytometry core Cyto-ICAN, Institute of Cardiometabolism and Nutrition, Hôpital Pitié-Salpêtrière, Paris, France

6. Service de Pneumologie et Soins Intensifs Respiratoires, Hôpital de Bicêtre, Assistance Publique Hôpitaux de paris, Le Kremlin Bicêtre, France.

7. Laboratoire CarMeN, UMR INSERM U1060/INRA U1397, Université Claude Bernard Lyon1, F-69310 Pierre-Bénite and F-69500 Bron, France.

#. Present address LRTOX, IRSN, 31 avenue de la division Leclerc, 92260 Fontenay aux Roses

** Equally contributing authors*

Correspondence to : florent.soubrier@sorbonne-universite.fr

Abstract

Hereditary pulmonary veno-occlusive disease (hPVOD) is a severe form of autosomal recessive pulmonary hypertension and is due to biallelic loss-of-function of the *EIF2AK4* gene (alias *GCN*2) coding for GCN2. GCN2 is a stress kinase that belongs to the integrated stress response pathway (ISR). Three rat lines carrying biallelic *Gcn2* mutation were generated and found phenotypically normal and did not spontaneously develop a PVOD-related disease. We submitted these rats to amino acid deprivation to document the molecular and cellular response of the lungs and to identify phenotypic changes that could be involved in PVOD pathophysiology. *Gcn2*$^{-/-}$ rat lungs were analyzed under basal conditions and three days after a single administration of PEG-asparaginase (ASNase). Lung mRNAS were analyzed by RNASeq and single cell RNASeq (scRNA-seq), flow-cytometry, tissue imaging, and western-blots. The ISR was not activated after ASNase treatment in *Gcn2*$^{-/-}$ rat lungs, and apoptosis was increased. Several proinflammatory and innate immunity genes were overexpressed, and inflammatory cells infiltration was also observed in the perivascular area. Under basal conditions, scRNA-seq analysis of *Gcn2*$^{-/-}$ rat lungs revealed increases in two T cell populations, a LAG3^{+} T cell population and a proliferative T cell population. Following ASNase administration, we observed an increase in calprotectin expression involved in TLR pathway activation and neutrophil infiltration. In conclusion, under basal and asparagine and glutamine deprivation induced by asparaginase administration, *Gcn2*$^{-/-}$ rats display molecular and cellular signatures in the lungs that may indicate a role for *Gcn2* in immune homeostasis and provide further clues to the mechanisms of hPVOD development.

INTRODUCTION

Pulmonary veno-occlusive disease (PVOD) is a rare and severe lung disease characterized by pulmonary vascular remodeling. Vascular remodeling involves small veins and venules with intimal fibrosis and medial hypertrophy, muscular hyperplasia of interlobular septal veins, and arterial remodeling illustrated by profound media hypertrophy of small arteries[1,2]. As lumen diameter decreases, pulmonary vascular resistance increases and thus leads to progressive right ventricular failure.

PVOD presents either as a sporadic disease, occurring late in life and favored by tobacco consumption, occupational exposure to organic solvents and alkylating agent treatment, or as a hereditary form[3–5]. The hereditary form (hPVOD) is due to pathogenic variants present in the *EIF2AK4* gene (also known as and hereinafter as General Control Nonderepressible 2, *GCN2*) rendering both alleles nonfunctional. hPVOD is inherited in an autosomal recessive manner with near complete penetrance, although the age of disease onset may vary, occurring from birth until 50 years of age[6]. Lung histology of biallelic *EIF2AK4* mutation carriers differs from non-carriers by significantly more severe intimal fibrosis, less pronounced medial hypertrophy, and marked muscular hyperplasia of interlobular septal veins[7]. The relationship between *GCN2* gene deficiency and pulmonary disease development remains unknown, as no clear links between gene function and the pathological lung lesions have yet been identified. The GCN2 protein is known to have a central role in sensing and responding to amino acid deficiency by shutting down protein translation, a mechanism common to all mammalian cells[8]. During cellular conditions of amino acid starvation, the cytoplasmic kinase GCN2 binds uncharged tRNAs with high affinity and is then activated by dimerization and autophosphorylation [9]. GCN2 may have additional role apart from amino acid sensing, since we recently demonstrated that loss of GCN2 specifically in hPVOD, induces pulmonary lipointoxication, a pathological process not seen in sporadic PVOD [10].

To decipher the mechanisms linking amino acid deficiency sensing and PVOD development, we interrupted *Gcn2* function in Sprague-Dawley rats by introducing small gene deletions using CrispR-CAS9 genome editing technology. In contrast to humans carrying *GCN2* biallelic mutations, homozygous *Gcn2*-deficient

rats do not develop PVOD, either spontaneously or in response to various stresses, as previously observed in *Gcn2* mutant mice. *Gcn2*-deficient rats are, however, exquisitely sensitive to acute asparagine and glutamine deprivation induced by asparaginase administration, in contrast to wild-type rats. We therefore analyzed changes in mRNA expression and cell populations in the lungs of wild-type and *Gcn2*-deficient rats. Our results highlight the critical role of GCN2 in both the pulmonary inflammatory response and T cell proliferation.

METHODS

In vivo study design - *Gcn2*- (alias *Eif2ak4*) deficient rats were generated on a Sprague Dawley background using the CrispR-CAS9 method as previously described[11]. Briefly, a frameshift deletion was introduced in the first exon of the *Gcn2* gene to disrupt the gene. We developed three lines with biallelic deletions of 152 bp, 41 bp, and 25 bp; designated $Gcn2^{152-/-}$, $Gcn2^{41-/-}$ and $Gcn2^{25-/-}$, respectively. Three-week-old rats were genotyped using genomic DNA obtained from ear punches as described in Manaud *et al.*[11]. PCRs were performed using 5X Herculase, and primers were designed to encompass mutant sequences (UPTE71-EIF2AK4: 5'-GAGGTCCCGTTTTCAGAGC-3' and LoTE71-EIF2AK4: 5'-AAGTCGAGGTGGGGAAGAAT-3'). Eight- to ten-week-old male and female rats weighing approximately 400 g were randomly assigned to receive either an intramuscular injection of 75 U/kg PEG-asparaginase (ASNase; Oncaspar, Shire) or an equal volume of vehicle (Vhcl; 0.9% NaCl). Because ASNase induces dramatic weight loss in *Gcn2* mutant rats, animals were euthanized three days post-injection (corresponding to a 20% weight loss threshold). Blood and organs were collected for histological and molecular studies. Two lung lobes from each animal were inflated with OCT and either frozen in isopentane on liquid nitrogen or fixed in paraformaldehyde for 72 hours. Remaining lobes were flash-frozen in liquid nitrogen.

Histopathology – Paraformaldehyde-fixed histological samples were embedded in paraffin, and serial sections of 5 µm were obtained from lung tissues. Sections were stained with hematoxylin-

eosin (HE) staining. Lung samples from all rats were retrospectively analyzed in a blinded fashion by conventional light microscopy.

Western blots **–** Proteins from rats' lung tissue were extracted in lysis buffer containing 1% Igepal®, 20 mmol/L Tris-HCl, 137 mmol/L NaCl, 10% glycerol, 2 mmol/L EDTA, 1 mmol/L Na3VO4, leupeptin 10 µg/µL, pepstatin 10 µg/µL, aprotinin 10 µg/µL, and a protease- inhibitor cocktail (aprotinin, leupeptin, and Pefabloc® [Roche]). A total of 50 µg of protein were separated on SDS-PAGE and transferred to nitrocellulose membrane. After blocking, membranes were incubated in 5% BSA in TBS 0.1% Tween-20 overnight at 4°C with primary antibodies –described in the Table E4. Blots were incubated with horseradish peroxidase (HRP)-conjugated goat anti-mouse diluted 1:1000 (Bio-techne) or with HRP-conjugated goat anti-rabbit diluted 1:1000 (Bio-techne). Immuno-reactive bands were revealed using ECL reagents (Biorad). Image-J Software was used to quantify the level of protein expression.

Immunofluorescence labeling (calprotectin, CD3, Ki67 and CD11b) – Rat lungs were inflated by intratracheal injection of 4-6 ml Optimal Cutting Temperature (Leica, 50% in PBS) and were immersed in isopentane, frozen in liquid nitrogen, embedded in O.C.T and stored at -80°C. Cryosections of 10 µm thickness were fixed in formalin (10 min at RT). They were then permeabilized in methanol/acetone (1:1) (10 min at -20°C). Nonspecific binding was blocked with 5% bovine serum albumin (BSA) and 10% goat serum in PBS (1 h at RT) and sections were incubated with primary antibodies diluted in 5% BSA and 3% goat serum described in Table E4 overnight at 4°C. Secondary antibodies (anti-mouse or anti-rabbit fluorophore-coupled, depending on the antigen tested) were diluted in 5% BSA and 3% goat serum and incubated 1 h at room temperature (RT). Immunolabeled sections were mounted with Dako fluorescent mounting medium (Dako) and examined under a confocal microscope (Leica SPE confocal microscope). Control sections were stained by omitting primary antibodies and did not show labeling. For

positive cell counting, images were analyzed by an investigator blinded to the experimental status of animals. A total of 20 to 40 fields were analyzed per animal. Images were analyzed using NIH ImageJ. Control experiments were performed using secondary antibody alone and showed no non-specific labeling.***RNA preparation and RNAseq analysis -*** Frozen lung samples were processed to obtain high-quality RNA for RNA Sequencing (RNAseq). A detailed protocol is provided in supplemental data. Final pooled sample libraries were sequenced on the Novaseq 6000 ILLUMINA, generating 2 x 5.10^7 paired-end base reads per sample after demultiplexing. Bioinformatic analyses were performed at the Paris ICM Institute's Data Analysis Core (iconics.institutducerveau-icm.org/). Data were normalized with DESeq2 (v1.26.0) bioconductor packages, prior to differential analysis with the DESeq2 workflow. Multiple tests-adjusted p-values were calculated with the Benjamini-Hochberg procedure to control FDR. Finally, enrichment analysis was conducted using Hallmark databases and KEGG pathways with the clusterProfiler R package (v3.14.3) with Gene Set Enrichment Analysis.

Single-cell RNAseq - For every experimental group, three female rats from each KO line: *Gcn2*$^{152-/-}$, *Gcn2*$^{41-/-}$, and *Gcn2*$^{25-/-}$ were euthanized and exsanguinated. Lungs were inflated with enzymatic solution (1.76 U/ml dispase, 0.15 U/ml collagenase) and slowly stirred at 37°C for 1 hour in 20 ml of enzymatic solution. Following digestion, lungs were pooled and cells were mechanically dissociated by carefully mincing into small pieces (2 to 3 mm^3). The resulting cell suspension was filtered through a 70-micron sieve in order to eliminate cellular debris, then red blood cells were lysed. After washing, viable cells were selected by cell sorting using Zombie-green (Biolegend). SingleCell library prep were performed with chromium from 10X Genomics. Chromium Next GEM Single Cell 3' GEM kit and Chip G were used, following the manufacturer's recommendations. A total of 5,000 to 20,000 cells were loaded onto chromium and sequenced on the Novaseq 6000 ILLUMINA. Using a 100-cycle ILLUMINA cartridge, calculations were based on a minimum of 20,000 reads/cell per sample. Cell assignments were performed based on known cell-type marker genes. Most of the cell-type marker genes used in the identification come from published data[12–14]. Detailed bioinformatic methods are described in supplemental data.

T cell characterization by flow cytometry - Rats were euthanized and after exsanguination, lungs were washed in cold PBS and cut into small pieces (2–3 mm^3). The multi-Tissue Dissociation Kit 2 (Miltenyi biotec) was used in combination with the gentle MACS Dissociator (Miltenyi biotec) according to the manufacturer's instructions. Tissues were passed through a 70-µm cell strainer and washed in 5% HBSS-BSA. Cells were then incubated for 1 min with red blood cell lysis buffer (RBCL, Invitrogen). Isolated rat lung cells were surface stained for 10 min on ice in the dark. Antibodies used were CD3 Viobright B515, CD4 PerCPVio700, and CD8b APC-Vio770. Viability Fixable Dye Vioblue (Miltenyi biotec) was used on lung cells as a viability cell marker. All the antibodies are described in Table E4. After 30 min fixation with 1% paraformaldehyde, cells were washed with PBS and centrifuged for 5 min at 300g at 4°C. We realized 20 min of permeabilization (0.15% saponin in PBS), and then stained with LAG3 conjugated with PE (phycoerythrin). After washing twice with PBS, all stained cells were resuspended in PBS and acquired by flow cytometry using a MACSQUANT 10 (Miltenyi Biotech) and the results analyzed on FLOWJO software. Fluorescence compensation was performed with single-stained cells and unstained cells. FMO (Fluorescence Minus One) controls were used in all experiments to gate positive staining. Forward scatter (FCS) and side scatter (SSC) profiles allowed the exclusion of debris and doublets. Dead cells were excluded based on the Fixable Dye Vioblue. Analysis was performed on live single cell population (Figure E7).

Cytokines measurements in rat plasma. Plasmas were isolated from 4-6 rats, wild-type rats and *Gcn2*$^{-/-}$ rats, treated or not treated by ASNase (3 days). Multiplex measurement of cytokines was performed using the rat R&D systems Luminex discovery assay that includes 17 cytokines (ref LXSARM), R&D system (listed in supplemental information).

RESULTS

Gcn2$^{-/-}$ rat phenotype under basal and stress conditions

After more than 12 months of observation by echocardiography and lung sections morphometry analyses, *Gcn2*$^{-/-}$ rats did not develop spontaneous PVOD nor any other obvious phenotype. Baseline parameters including weight, Doppler echocardiography parameters, Fulton index are normal as compared to control rats in the 3 lines of *Gcn2* deficient rats (see supplemental material, table E1).

Attempts to induce the disease using known GCN2 function-related stresses (intra-uterine growth retardation, hypoxia, LPS-induced inflammation) were unsuccessful (results not shown)[15].

Systemic responses to asparaginase in *Gcn2*$^{-/-}$ rats

Considering GCN2 is one of the main sensors of amino acid starvation in the organism, we injected asparaginase (ASNase) at a dose of 75 U/Kg in both wild-type and homozygous *Gcn2* KO rats in order to evaluate their response to amino acid deprivation in the presence or absence of functional GCN2. The chemotherapy agent ASNase depletes serum levels of asparagine and glutamine, starving cells of essential substrates, and induces GCN2 activation. ASNase treatment induced rapid weight loss in *Gcn2*$^{-/-}$ animals with health status deterioration, therefore experiments were stopped at three days post-injection (Figure 1A). In contrast, wild-type animals did not show any detectable physiological deterioration. Macroscopic observation of the organs from ASNase-treated *Gcn2*$^{-/-}$ animals revealed a yellowish liver, which upon microscopic examination, contained lipid droplets suggesting developing steatosis (Figure E1 in supplemental data). ASNase-induced asparagine and glutamine starvation was the only condition in which we observed a phenotypic difference between *Gcn2*-deficient and WT rats.

Asparaginase induced an integrated stress response (ISR) and autophagy in WT rat lungs and increased apoptosis in *Gcn2*$^{-/-}$ rat lungs.

ASNase treatment increased phospho-(T899)-GCN2 and total GCN2 protein in WT animals, neither of which was detected in *Gcn2*$^{-/-}$ rats (Figure 1B, B1-B2)[16]. Consistent with this result, ATF4 (Activating transcription factor 4), a downstream component of ISR, was significantly increased in ASNase-treated WT animals but remained unchanged in ASNase-treated *Gcn2*$^{-/-}$ animals (Figure 1C). Asparagine synthetase (Asns) and Sestrin-2 proteins, known transcriptional targets of ATF4, were also increased in ASNase-treated WT animals (Figure 1, B4 and C2). We measured the expression of another EIF2 kinase, PERK, which is activated by endoplasmic reticulum stress. PERK was significantly increased in WT rats treated with ASNase and was unchanged in ASNase-treated *Gcn2*$^{-/-}$ rats (Figure 1B). These results demonstrate that the integrated stress response (ISR) is activated in ASNase-treated WT animals but is not induced in *Gcn2*$^{-/-}$ animals. Given that the downstream autophagy pathway is triggered by GCN2-induced-ISR during amino acid starvation and/or inflammatory stress[17,18], we therefore assessed autophagy using four different protein markers; p62, LC3B and ATG3. ATG3 and p62 increased with ASNase treatment in WT rats as compared *to Gcn2*$^{-/-}$ rats, whereas LC3B remained stable in both WT and *Gcn2*$^{-/-}$ rats following ASNase treatment (Figure 2A). In summary, in contrast to WT rats, ISR and autophagy were not induced in *Gcn2*$^{-/-}$ rats in response to asparagine and glutamine deprivation.

Lung cell apoptosis was significantly increased in *Gcn2*$^{-/-}$ rats as compared to WT rats after ASNase treatment, as measured by TUNEL. In contrast, there was no difference at basal conditions (Figure 2B).

RNAseq experiments reveal whole lung inflammation in ASNase-treated *Gcn2*$^{-/-}$ rats.

We performed RNAseq transcriptome analysis to document the lung response to ASNase-induced amino acid deprivation in both WT and *Gcn2*-deficient rats. Results were compared with those from *Gcn2*$^{-/-}$ and WT rats treated with vehicle (NaCl 0.05%, Vhcl) corresponding to basal conditions. Under basal conditions, only a few genes were differentially regulated between *Gcn2*$^{-/-}$ and WT rats, consistent with the absence of

phenotypic abnormalities in KO rats. Expression analysis showed 680 differentially upregulated and 628 differentially downregulated genes between *Gcn2*$^{-/-}$ ASNase and WT ASNase groups (Figure 3, A-C).

In order to identify which gene networks were altered during ASNase treatment, differentially expressed genes (DEGs) were investigated using the Gene Set Enrichment Analysis (GSEA) algorithm based on the Hallmark collection of Molecular Signature Database (MSigDB). This analysis revealed a number of significantly upregulated genes related to inflammation (Figure 3D), e.g., *Nfkb2* (Hallmark geneset: TNF-α signaling via NF- κB), *Ccl2* (encoding MCP-1), *Il6*, *Il1b*, *Sele* coding for E-selectin (Hallmark geneset: inflammatory response), and *Myd88* (Hallmark geneset: interferon gamma response). These genes found to be upregulated with RNAseq in ASNase-treated *Gcn2*$^{-/-}$ rats were confirmed with qPCR (Figure 4, A-F). In addition, the Hallmark geneset inflammatory response gene heatmap illustrated that inflammatory genes were uniquely overexpressed in ASNase-treated *Gcn2*$^{-/-}$ rats (Figure 3C). Calprotectin is synthesized by innate immune cells, such as neutrophils, monocytes and macrophages. The two calprotectin subunits are encoded by the *S100a8* and *S100a9* genes whose expression were more than 30-fold increased in ASNase-treated *Gcn2*$^{-/-}$ rats (Table E2), a result consistent with the significant increase in serum calprotectin levels as determined by ELISA (Figure 4G) and in lung section by immunofluorescence (Figure E2). Calprotectin is a known damage-associated molecular pattern (DAMP) component, able to activate toll-like receptors (TLR) by an autocrine mechanism [19]. Indeed, we observed increased expression of *Tlr-2*,*-9*, *-10* and-*11* in ASNase-treated *Gcn2*$^{-/-}$ rats (Table E2). *Myd88*, one of the most upregulated genes, codes for a cytosolic adaptor protein linking activated Toll-like receptors with other intracellular signaling intermediates. Altogether, these results demonstrate upregulation of the TLR-MYD88 pathway genes. Inflammation is also detected at the histological level. Interstitial edema and inflammatory cell infiltration are observed in the lungs of *Gcn2*$^{-/-}$ rats treated with ASNase. This cell infiltration is composed of inflammatory cells and appears to be predominantly perivascular. These inflammatory lesions are not observed in ASNase-treated WT rats (Figure E3).

Identification of cell populations in whole rat lung tissue by scRNA-seq.

scRNA-seq was performed on pooled samples of three lungs from each KO line (*Gcn2*$^{152-/-}$, *Gcn2*$^{41-/-}$ and *Gcn2*$^{25-/-}$) in order to neutralize any potential off-target events inherent to CrispR-CAS9 technology. A single pool of animals was analyzed per experimental group (*Gcn2*$^{-/-}$ ASNase, WT ASNase, *Gcn2*$^{-/-}$ Vhcl, and WT Vhcl). All sequencing experiments passed quality control steps (Figure E4). A total of 18,201 cells were analyzed and a median 1341 genes were detected per cell. mRNA expression clustering enabled us to identify 19 distinct cell populations (Figure 5A). Each cell population was characterized by the expression of known markers (Figure 5B). Cell clusters correspond to three cell families: epithelial cells, immune cells, and vascular cells (Figure 5C). In the epithelial cell group we observed club cells and a rare population of Tuft cells, also known as brush cells, which were characterized by *Dclk1* and *Lrmp* expression[20,21]. The vascular wall cell group was composed of endothelial cells, smooth muscle cells, and fibroblasts. Interestingly, ASNase treatment increased endothelial cell number only in WT rats, whereas fibroblasts were increased in *Gcn2*-deficient rats as compared to the other experimental groups. Immune cell numbers also underwent significant changes. In the myeloid lineage, neutrophils and classical monocytes were strongly increased in ASNase-treated *Gcn2*$^{-/-}$ rats, and non-classical monocytes were also increased to a lesser extent. Two populations of T-lymphoid cells expressing CD3 were unexpectedly increased under basal conditions in *Gcn2*$^{-/-}$ rats. One population was characterized by predominant expression of the *Lag3* gene, encoding an inhibiting receptor of T cells (T_LAG3 cells) (Figure 5C and Table E6). This population included CD4^{+} and CD8^{+} T cells, and was only observed in untreated *Gcn2*$^{-/-}$ rats, and disappeared with ASNase treatment. Another T cell population was also increased in *Gcn2*$^{-/-}$ rats under basal conditions but did not express *Lag3*. This population was shown to be in a proliferating state as attested by increased ki67 expression.

ScRNA-seq experiments highlight cell population-specific gene and pathway regulation.

Differentially expressed genes (DEGs) were analyzed across cell populations identified through scRNAseq. This analysis revealed genes whose differential expression was specific to an experimental condition and/or

a particular cell type. Under basal conditions, only T_LAG3 and endothelial cell populations displayed a large number of DEGs between *Gcn2* mutant and WT rats. In contrast, under ASNase conditions, most of the individual cell populations exhibited high numbers of DEGs between the two genotype groups (Figure 6A). Several gene modulations were detected in endothelial cells of *Gcn2*$^{-/-}$ rats under basal conditions. Indeed, *Bmpr2*, the major predisposing gene for PAH, was upregulated in endothelial cells from *Gcn2*$^{-/-}$ rats. *Eng*, encoding the vascular endothelium glycoprotein endoglin, and *Il33*, encoding an interleukin involved in immune cell activation, were also exclusively upregulated in endothelial cells from the *Gcn2*$^{-/-}$ Vhcl group (Figure 6B). In endothelial cells from ASNase-treated *Gcn2*$^{-/-}$ rats, one of the most upregulated genes was leucine-rich-alpha2-glycoprotein, *Lrg1* ($p=1.37x10^{-4}$, logFC=1.33; Figure 6B). LRG1 belongs to the leucine-rich repeat family of proteins involved in protein-protein interaction, and to the TGF-β signaling pathway. In T_LAG3 cells, *Gata3*, a transcription factor involved in T cell development, proliferation, and maintenance, was exclusively upregulated in the *Gcn2*$^{-/-}$ Vhcl group (Figure 6B). Interestingly, DEG pathway enrichment analysis from the T_LAG3 population revealed downregulation of ribosomes machinery and the mRNA transport pathway in *Gcn2*$^{-/-}$ compared to WT rats under basal conditions (Table E3). Following ASNase treatment, *Ddit3* and *Atf3* genes were exclusively upregulated in neutrophils of WT but not of *Gcn2*$^{-/-}$ rats, indicating absence of ISR activation in the latter (Figure 6B).

Flow-cytometry analysis and immunofluorescence imaging confirm cluster identification and differential regulation.

The T_LAG3 population found only in *Gcn2*$^{-/-}$ rats under basal conditions was confirmed by flow cytometry analysis. Using whole lungs from an additional set of *Gcn2*$^{-/-}$ Vhcl and WT Vhcl rats (n=5/group), we analyzed cells to validate the increase in T_LAG3 cells in *Gcn2*$^{-/-}$ rats under basal conditions observed by scRNAseq. We used the CD3 cell surface marker to identify the global T cell population. CD4 and CD8 cell surface markers were added to determine the proportion of $LAG3^+$ T cells in $CD3^+/CD4^+$ and $CD3^+/CD8^+$ T cell populations. Finally, we used the LAG3 marker to investigate the T_LAG3 population

(Figure E7). Interestingly, we observed that the increase in LAG3 marker expression was essentially intracellular (for either condition there was no signal without permeation). Furthermore, the percentage of $CD3^+/LAG3^+$ cell populations was significantly increased in *Gcn2*$^{-/-}$ rats under basal conditions as compared to WT, thus confirming our scRNAseq results (Figure 7A). The percentage of $LAG3^+$ cells tended to increase in both $CD3^+/CD4^+$ and $CD3^+/CD8^+$ populations (p=0.09; Figure 7A). Flow cytometry analysis demonstrated that the LAG3 increase appeared to be mainly detected within the intracellular compartment, suggesting that the T_LAG3 population remains in an unstimulated state in *Gcn2*$^{-/-}$ rats under basal conditions. T cell proliferation was assessed by double labeling with CD3 and Ki67 antibodies followed by immunofluorescence (IF) analyses. A two-fold increase in dual-positive cells illustrated greater T cell proliferation in *Gcn2* $^{-/-}$ rats under basal conditions (Figure 7B).

The significantly increased expression of *S100a8* and *S100a9* genes encoding calprotectin subunits suggested an increase in classical monocyte and neutrophil populations as supported by scRNAseq. IF double-staining using CD11b, as marker of myeloid cells, and calprotectin antiserum showed an increase in calprotectin expressing myeloid cells during ASNase treatment in *Gcn2* deficient rats (Figure 8 A-B et Figure E2). Western blot experiments further demonstrated that MMP9, a metalloprotease expressed in neutrophils was increased in ASNase-treated *Gcn2*$^{-/-}$ rats (Figure 8C).

Cytokine measurements in rat plasma.

Among seventeen cytokines measured in the plasma of experimental rats of both genotypes, we observed a significant increase in CXCL3, ICAM-1, TIMP1, VEGF, IL-18 and Il-6 in *Gcn2* deficient rats treated by ASNase, as compared to the other experimental groups (Figure 9).

Altogether, these results demonstrate an active inflammatory state in *Gcn2* deficient rats involving both T-lymphocyte dysregulation in basal conditions and innate immunity activation in under amino acid deprivation in *Gcn2*$^{-/-}$ rats.

DISCUSSION

We generated genetically *Gcn2*-deficient rats by CrispR-CAS9 to create an animal model of heritable PVOD. These rats, as well as *Gcn2* KO mice, do not develop spontaneous PVOD, even after twelve months. To induce a state of amino acid deprivation, a relevant condition for GCN2 activation, we used asparaginase, an anti-leukemia drug that causes asparagine and glutamine deficiency. We found this treatment to be the only experimental condition that strongly discriminated between WT and *Gcn2*$^{-/-}$ rats since *Gcn2* mutant rats underwent rapid weight loss with fatal consequences within a few days of administration, whereas WT rats did not show any significant physiological failure.

We conducted transcriptomic profiling and scRNAseq in *Gcn2*$^{-/-}$ and WT rat lungs three days after a single ASNase injection to gain insight into the molecular and cellular responses to this stress.

Under basal conditions, only five genes were differentially regulated, consistent with the absence of phenotypic alterations in *Gcn2*-deficient rats. However, *Gcn2*-deficient rat lungs contained large populations of T_LAG3 cells expressing LAG3 (CD223), a key member of the immunoglobulin superfamily and a CD4 paralog that binds MHC class II molecules with very high affinity and has an intrinsic negative regulatory T cell function by its role as an immune checkpoint receptor [22]. Other studies have shown that persistent antigen exposure results in sustained LAG3 expression and contributes to a state of "exhaustion" responsible for impaired proliferation of T cells and decreased cytokine production[23]. Previous reports have demonstrated that LAG3 is mainly localized in the intracellular compartment and is translocated to the cell surface upon stimulation[24]. Using flow cytometry, we confirmed that LAG3 had intracellular localization in this T cell population from *Gcn2*$^{-/-}$ rats under basal conditions. Under unstimulated conditions, the majority of LAG3 does not reach the cell surface and likely undergoes degradation within lysosomal compartments[24]. Nevertheless, DEGs analysis of T_LAG3 cells highlighted increased *Lag3* expression in *Gcn2*$^{-/-}$ compared to WT rats under basal conditions. Given that intracellular LAG3 is accumulating in these *Gcn2*$^{-/-}$ rats, the degradation pathway might be unable to clear the increased LAG3 expression.

Interestingly, the T_Prolif cell population also increased in *Gcn2*$^{-/-}$ rats under non-stimulated conditions. Considering that this cell population expresses LAG3 at higher level in *Gcn2* deficient rats, it is possible that T_LAG3 cells are proliferating at higher rates than in WT animals. Moreover, the T_LAG3 expressing cell population is no longer detected after ASNase treatment and T_Prolif also decrease under ASNase treatment. It has been previously shown that T cells ($CD4^+$, $CD8^+$, and $CD4^+/CD8^+$), B cells ($B220^+$ $sIgM^+$), and leukocytes ($CD11b^+$) from *Gcn2*$^{-/-}$ mice display enhanced cell death when exposed to ASNase-induced amino acid deficiency[25]. Considering that GCN2 and amino acid supply are both necessary for T cell survival and differentiation, we can suppose that GCN2-deficient T_LAG3 and the subpopulation of T_prolif expressing LAG3 cells undergo cell death with ASNase treatment [26].

Since GCN2 has been reported to play a role in immune cell differentiation[27,28], it is possible that *Gcn2*-deficient T cells cannot differentiate as efficiently as WT T cells during asparagine and glutamine starvation induced by ASNase treatment. Indeed, we found that the T_Eff population, corresponding to activated T cells, was significantly decreased in *Gcn2*$^{-/-}$ rats compared to WT rats after ASNase treatment, whereas T_Naïve populations, corresponding to quiescent T cells, remained unchanged between experimental groups. Moreover, instead of being necessary for T cell proliferation, as proposed by Munn *et al.*[29], Van de Velde *et al.* suggested that GCN2 is required for normal cytotoxic T_Eff function. The possible inability of T_Eff to lyse activated antigen presenting cells could be one cause of the increased inflammatory status observed under amino acid starvation conditions.

Altogether, GCN2 loss of function impedes normal T cell development and leads to their proliferation, resulting in an increased T_LAG3 population that is unable to survive when rats are undergoing metabolic stress. ASNase treatment affects GCN2-deficient T cell differentiation, resulting in decreased T_Eff populations, and, possibly, cytotoxic dysfunction.

GCN2 has already been demonstrated as critically important in limiting ASNase toxicity in the liver and pancreas in rodents [30,31]. Consistent with these results, cytosolic vacuoles were present in yellowy livers from ASNase-treated *Gcn2*$^{-/-}$ rats, suggesting steatosis and inflammation. Indeed, ASNase treatment rapidly led to severe morbidity in GCN2-deficient rats indicating a high sensitivity to asparagine and glutamine

depletion. We cannot exclude the possibility that inflammatory mediators originating from other organs, such as the liver or intestine, could target the lungs and indirectly induce lung injury.

As previously described in mice, we confirm that the GCN2 protein kinase is required to activate integrated stress responses in rats treated with ASNase. In accordance with the previous observation that ISR failure can drive cells towards apoptosis[25], we showed that apoptosis increased in lung cells from ASNase-treated *Gcn2*-deficient rats using the TUNEL assay. Given that there is growing evidence that cell death can activate the immune response either by antigens transfer to the immune system or by DAMPs release[32,33], we speculate that increased cell death is an inflammatory trigger in ASNase-treated *Gcn2*-deficient rats. Ravishankar *et al.* demonstrated the important role of GCN2 in regulating the tolerogenic response to apoptotic cell antigens by inducing IL-10 and TGF-β production in macrophages[34]. We detected the DAMP molecule calprotectin, whose two subunits are encoded by the *S100a8* and *S100a9* genes that were both strongly overexpressed in the lung of ASNase-treated GCN2 deficient rats and increased in their serum. Several reports have suggested that the immune system senses cell death via the TLR2 and/or TLR9 pathway(s)[35]. In fact, DAMP molecules, such as calprotectin, can either activate the TLR pathway in sentinel cells (macrophages and mast cells) or in an autocrine manner via neutrophils[36,37]. This data, along with our current results demonstrating *Tlr2*, *Myd88*, *Il6*, and *Il1B* overexpression, collectively suggest that the observed increased cell death could be responsible for increased inflammation processes by releasing calprotectin and inducing TLR pathway activation. Calprotectin is involved in neutrophil migration to inflammatory sites[38] and its increased expression in *Gcn2* mutant rats correlates with the increased CD11b myeloid cell population as attested by scRNAseq and immunofluorescence analysis of lung cells. Interestingly, the parallel increased expression of MMP9, known to promote revascularization at injury sites[39], could suggest a possible role for neutrophils in vascular remodeling. It was previously shown that neutrophils facilitate monocyte recruitment, likely explaining increased numbers of monocytes in ASNase-treated *Gcn2*$^{-/-}$ rats[40]. Finally, inflammation activation could also be due to defective autophagy in *Gcn2*$^{-/-}$ rats. Ravindran *et al.* found an enhanced inflammatory response in the gut of *Gcn2*$^{-/-}$ mice following dextran sodium sulfate (DSS) administration that was imputed to decreased autophagy activation[18]. Consistent with

their results, we found that autophagy, as evaluated on key proteins of this pathway, was not induced in ASNase-treated *Gcn2*$^{-/-}$ rats in contrast to WT.

Endothelial cells (ECs) play a major role in vascular remodeling and several genes of interest were strongly modulated in this cell population. We observed a major increase in *Lrg1* gene expression in ASNase-treated *Gcn2*$^{-/-}$ mutant rats. LRG1 is mitogenic for endothelial cells in the presence of TGF-β1 and induces angiogenesis. Owing to its interaction with endoglin, LRG1 increases endothelial TGF-β type II receptor and ALK1 activation and signaling by activating the Smad1/5/9 pathway[41]. More recently, Singhal *et al.* showed that LRG1 increased the number of NG2^{+} perivascular cells[42]. *Lrg1* upregulation in lungs from *Gcn2*-deficient rats under stress conditions might offer a clue to understanding the large ECs proliferation conferring a capillary hemangiomatosis aspect observed in some patients with hPVOD. LRG1 is also expressed in neutrophils where emerging data suggest that LRG1 plays a role in innate immunity [43]. *BMPR2* and *endoglin*, two genes involved in BMP signaling in endothelial cells and linked to hereditary predisposition to PAH development, were found upregulated in endothelial cells from *Gcn2* mutant rats under basal conditions. These two gene overexpressions may represent a compensatory mechanism to cope with the BMP/TGFb imbalance found in hPVOD. Indeed, we already published that phosphorylation of SMAD1/5/9, the downstream signaling below BMPR2, is strongly reduced in human hPVOD, but also in mitomycin C (MMC)-induced PVOD in rats, without significant alteration of BMPRII protein expression [11,44]. We also relevantly demonstrated that the pulmonary phosphorylation of SMAD1/5/9 is specifically reduced in our *Gcn2*$^{-/-}$ rats and that pharmacological or siRNA-based inhibition of GCN2 negatively regulates BMP-dependent SMAD1/5/9 signaling in pulmonary endothelial cells, in part through modulation of chordin [11]. Loss of GCN2 enhances as well the mRNA levels of collagen I by decreasing ATF3-dependent p38 phosphorylation, which promotes the collagen I synthesis in PASMCs and eventually leads to increased collagen deposition in the pulmonary artery wall [45]. Accordingly, vascular remodeling and pulmonary fibrosis are aggravated in a model of group 3 PH induced by bleomycin in our *Gcn2*$^{-/-}$ rat, potentially through an IL-6-dependent mechanism [46]. The fact that we found an increased number of fibroblasts in the lungs of *Gcn2*-deficient rats, and that biallelic *EIF2AK4* mutation carriers have

significantly more severe intimal fibrosis, support further the profibrotic influence of GCN2 loss-of-function [7]. Our results also suggest an activation of endothelial cells through IL-6 and E-selectin as RNAseq revealed that their transcripts were increased. E-selectin increase in endothelial cells mediates leukocyte rolling along the activated endothelium, neutrophil chemoattraction, and capture likely participating to neutrophil recruitment in *Gcn2* deficient rats [47,48]. Increased plasma levels of VEGF, CXCL3, IL-6 and IL-18 illustrate the angiogenic and proinflammatory status of *Gcn2* deficient rats treated by ASNase and corroborate results found at the expression levels in lung tissue.

There are some limitations to our study that must be discussed. The first is the absence of PVOD development in *Gcn2*-deficient rats, which prevented the observation of the molecular and cellular events associated with vascular remodeling. The scRNAseq experiments might have been biased because rare cell population, like cells progenitors for example, can be difficult to extract and included in the analysis. However, we conducted the study in accordance with standard protocols for lung experiments. Finally, although some gene modulations were integrated into gene networks likely involved in the ASNase treatment stress response in *Gcn2*-deficient rats, in view of severe physiological consequences, other gene alterations could be secondary to non-lung tissue failures, and may be difficult to interpret. Therefore, either there was an integrated regulatory system present that we have not yet identified, or several genes were increased due to compromised systemic physiological status. The *Gcn2*-deficient rodent model is characterized by a major difference compared with human subjects carrying biallelic *GCN2* deficiency, because severe PVOD usually occurs early in life, even in neonates, despite the absence of an identifiable trigger. We cannot eliminate a specific and unidentified inducing factor involved in humans to which the experimental rats have not been exposed, although we used several conditions to attempt to induce PVOD. Another hypothesis could refer to a specific inflammatory factor involved in the development of vascular remodeling in humans, which could be absent in rodents.

Interestingly, the whole lung RNAseq analysis did not allow the discrimination of molecular and cellular differences between WT and *Gcn2-/-* rats at the basal level, whereas scRNAseq, flow cytometry, and IF

staining on isolated pulmonary cells did. This demonstrates that the GCN2 loss-of-function can impact discrete circulating and/or resident pulmonary cells with subsequent effects on the pulmonary vasculature. Our results suggest that the activation of the lung's innate immune system in response to amino acid deprivation in *Gcn2*-deficient rats is the combination of calprotectin-induced TLR pathway activation associated with apoptosis-induced neutrophil recruitment and autophagy deficiency. Importantly, we propose a new role for GCN2 in adaptive immunity involving T cell development under basal conditions. These results suggest that GCN2 has an additional role to its amino acid sensor function that should be further investigated.

Acknowledgements : this work was supported by a grant from the Fondation de la Recherche Médicale (FRM) N° M18JRAS017

DOI for supplemental material : 10.6084/m9.figshare.22067858

REFERENCES

1. Montani D, Lau EM, Dorfmüller P, Girerd B, Jaïs X, Savale L, Perros F, Nossent E, Garcia G, Parent F, Fadel E, Soubrier F, Sitbon O, Simonneau G, Humbert M. Pulmonary veno-occlusive disease. *Eur Respir J*. 2016;47:1518–1534.

2. Mandel J, Mark EJ, Hales CA. Pulmonary Veno-occlusive Disease. *Am J Respir Crit Care Med*. 2000;162:1964–1973.

3. Ranchoux B, Günther S, Quarck R, Chaumais M-C, Dorfmüller P, Antigny F, Dumas SJ, Raymond N, Lau E, Savale L, Jaïs X, Sitbon O, Simonneau G, Stenmark K, Cohen-Kaminsky S, Humbert M, Montani D, Perros F. Chemotherapy-Induced Pulmonary Hypertension. *The American Journal of Pathology*. 2015;185:356–371.

4. Montani D, Lau EM, Descatha A, Jaïs X, Savale L, Andujar P, Bensefa-Colas L, Girerd B, Zendah I, Le Pavec J, Seferian A, Perros F, Dorfmüller P, Fadel E, Soubrier F, Sitbon O, Simonneau G, Humbert M. Occupational exposure to organic solvents: a risk factor for pulmonary veno-occlusive disease. *Eur Respir J*. 2015;46:1721–1731.

5. Montani D, Achouh L, Dorfmüller P, Le Pavec J, Sztrymf B, Tchérakian C, Rabiller A, Haque R, Sitbon O, Jaïs X, Dartevelle P, Maître S, Capron F, Musset D, Simonneau G, Humbert M. Pulmonary Veno-Occlusive Disease: Clinical, Functional, Radiologic, and Hemodynamic Characteristics and Outcome of 24 Cases Confirmed by Histology. *Medicine*. 2008;87:220–233.

6. Eyries M, Montani D, Girerd B, Perret C, Leroy A, Lonjou C, Chelghoum N, Coulet F, Bonnet D, Dorfmüller P, Fadel E, Sitbon O, Simonneau G, Tregouët D-A, Humbert M, Soubrier F. EIF2AK4 mutations cause pulmonary veno-occlusive disease, a recessive form of pulmonary hypertension. *Nature Genetics*. 2013;46:65.

7. Nossent EJ, Antigny F, Montani D, Bogaard HJ, Ghigna MR, Lambert M, Thomas de Montpréville V, Girerd B, Jaïs X, Savale L, Mercier O, Fadel E, Soubrier F, Sitbon O, Simonneau G, Vonk Noordegraaf A, Humbert M, Perros F, Dorfmüller P. Pulmonary vascular remodeling patterns and expression of general control nonderepressible 2 (GCN2) in pulmonary veno-occlusive disease. *J Heart Lung Transplant*. 2017;37:647–655.

8. Zhang P, McGrath BC, Reinert J, Olsen DS, Lei L, Gill S, Wek SA, Vattem KM, Wek RC, Kimball SR, Jefferson LS, Cavener DR. The GCN2 eIF2 Kinase Is Required for Adaptation to Amino Acid Deprivation in Mice. *Molecular and Cellular Biology*. 2002;22:6681–6688.

9. Masson GR. Towards a model of GCN2 activation. *Biochemical Society Transactions*. 2019;47:1481–1488.

10. Khoury S, Beauvais A, Colas J, Saint-Martin Willer A, Perros F, Humbert M, Vandebrouck C, Montani D, Ferreira T, Antigny F. Lipidomic Profile Analysis of Lung Tissues Revealed Lipointoxication in Pulmonary Veno-Occlusive Disease. *Biomolecules*. 2022;12:1878.

11. Manaud G, Nossent EJ, Lambert M, Ghigna M-R, Boët A, Vinhas M-C, Ranchoux B, Dumas SJ, Courboulin A, Girerd B, Soubrier F, Bignard J, Claude O, Lecerf F, Hautefort A, Florio M, Sun B, Nadaud S, Verleden SE, Remy S, Anegon I, Bogaard HJ, Mercier O, Fadel E, Simonneau G, Vonk Noordegraaf A, Grünberg K, Humbert M, Montani D, Dorfmüller P, Antigny F, Perros F. Comparison of Human and Experimental Pulmonary Veno-Occlusive Disease. *Am J Respir Cell Mol Biol*. 2020;63:118–131.

12. Hong J, Arneson D, Umar S, Ruffenach G, Cunningham CM, Ahn IS, Diamante G, Bhetraratana M, Park JF, Said E, Huynh C, Le T, Medzikovic L, Humbert M, Soubrier F, Montani D, Girerd B, Trégouët D-A, Channick R, Saggar R, Eghbali M, Yang X. Single-Cell Study of Two Rat Models of Pulmonary Arterial Hypertension Reveals Connections to Human Pathobiology and Drug Repositioning. *Am J Respir Crit Care Med*. 2021;203:1006–1022.

13. Guo M, Du Y, Gokey JJ, Ray S, Bell SM, Adam M, Sudha P, Perl AK, Deshmukh H, Potter SS, Whitsett JA, Xu Y. Single cell RNA analysis identifies cellular heterogeneity and adaptive responses of the lung at birth. *Nat Commun*. 2019;10:37.

14. Reyfman PA, Walter JM, Joshi N, Anekalla KR, McQuattie-Pimentel AC, Chiu S, Fernandez R, Akbarpour M, Chen C-I, Ren Z, Verma R, Abdala-Valencia H, Nam K, Chi M, Han S, Gonzalez-Gonzalez FJ, Soberanes S, Watanabe S, Williams KJN, Flozak AS, Nicholson TT, Morgan VK, Winter DR, Hinchcliff M, Hrusch CL, Guzy RD, Bonham CA, Sperling AI, Bag R, Hamanaka RB, Mutlu GM, Yeldandi AV, Marshall SA, Shilatifard A, Amaral LAN, Perlman H, Sznajder JI, Argento AC, Gillespie CT, Dematte J, Jain M, Singer BD, Ridge KM, Lam AP, Bharat A, Bhorade SM, Gottardi CJ, Budinger GRS, Misharin AV. Single-Cell Transcriptomic Analysis of Human Lung Provides Insights into the Pathobiology of Pulmonary Fibrosis. *Am J Respir Crit Care Med*. 2019;199:1517–1536.

15. Castilho BA, Shanmugam R, Silva RC, Ramesh R, Himme BM, Sattlegger E. Keeping the eIF2 alpha kinase Gcn2 in check. *Biochim Biophys Acta*. 2014;1843:1948–1968.

16. Romano PR, Garcia-Barrio MT, Zhang X, Wang Q, Taylor DR, Zhang F, Herring C, Mathews MB, Qin J, Hinnebusch AG. Autophosphorylation in the activation loop is required for full kinase activity in vivo of human and yeast eukaryotic initiation factor 2alpha kinases PKR and GCN2. *Mol Cell Biol*. 1998;18:2282–2297.

17. Battu S, Afroz S, Giddaluru J, Naz S, Huang W, Khumukcham SS, Khan RA, Bhat SY, Qureshi IA, Manavathi B, Khan AA, August A, Hasnain SE, Khan N. Amino acid starvation sensing dampens IL-1β production by activating riboclustering and autophagy. *PLoS Biol*. 2018;16:e2005317.

18. Ravindran R, Loebbermann J, Nakaya HI, Khan N, Ma H, Gama L, Machiah DK, Lawson B, Hakimpour P, Wang Y, Li S, Sharma P, Kaufman RJ, Martinez J, Pulendran B. The amino acid sensor GCN2 controls gut inflammation by inhibiting inflammasome activation. *Nature*. 2016;531:523–527.

19. Inciarte-Mundo J, Frade-Sosa B, Sanmartí R. From bench to bedside: Calprotectin (S100A8/S100A9) as a biomarker in rheumatoid arthritis. *Front Immunol*. 2022;13:1001025.

20. Zaragosi LE, Deprez M, Barbry P. Using single-cell RNA sequencing to unravel cell lineage relationships in the respiratory tract. *Biochem Soc Trans*. 2020;48:327–336.

21. Gerbe F, Brulin B, Makrini L, Legraverend C, Jay P. DCAMKL-1 Expression Identifies Tuft Cells Rather Than Stem Cells in the Adult Mouse Intestinal Epithelium. *Gastroenterology*. 2009;137:2179–2180.

22. Huo J-L, Wang Y-T, Fu W-J, Lu N, Liu Z-S. The promising immune checkpoint LAG-3 in cancer immunotherapy: from basic research to clinical application. *Front Immunol*. 2022;13:956090.

23. Andrews LP, Marciscano AE, Drake CG, Vignali DAA. LAG3 (CD223) as a cancer immunotherapy target. *Immunol Rev*. 2017;276:80–96.

24. Bae J, Lee SJ, Park C-G, Lee YS, Chun T. Trafficking of LAG-3 to the Surface on Activated T Cells via Its Cytoplasmic Domain and Protein Kinase C Signaling. *JI*. 2014;193:3101–3112.

25. Bunpo P, Cundiff JK, Reinert RB, Wek RC, Aldrich CJ, Anthony TG. The eIF2 Kinase GCN2 Is Essential for the Murine Immune System to Adapt to Amino Acid Deprivation by Asparaginase1–3. *The Journal of Nutrition*. 2010;140:2020–2027.

26. Van de Velde L-A, Guo X-ZJ, Barbaric L, Smith AM, Oguin TH, Thomas PG, Murray PJ. Stress Kinase GCN2 Controls the Proliferative Fitness and Trafficking of Cytotoxic T Cells Independent of Environmental Amino Acid Sensing. *Cell Rep*. 2016;17:2247–2258.

27. Sundrud MS, Koralov SB, Feuerer M, Calado DP, Kozhaya AE, Rhule-Smith A, Lefebvre RE, Unutmaz D, Mazitschek R, Waldner H, Whitman M, Keller T, Rao A. Halofuginone Inhibits TH17 Cell Differentiation by Activating the Amino Acid Starvation Response. *Science*. 2009;324:1334–1338.

28. Eleftheriadis T, Pissas G, Antoniadi G, Liakopoulos V, Tsogka K, Sounidaki M, Stefanidis I. Differential effects of the two amino acid sensing systems, the GCN2 kinase and the mTOR complex 1, on primary human alloreactive CD4+ T-cells. *International Journal of Molecular Medicine*. 2016;37:1412–1420.

29. Munn DH, Sharma MD, Baban B, Harding HP, Zhang Y, Ron D, Mellor AL. GCN2 Kinase in T Cells Mediates Proliferative Arrest and Anergy Induction in Response to Indoleamine 2,3-Dioxygenase. *Immunity*. 2005;22:633–642.

30. Wilson GJ, Bunpo P, Cundiff JK, Wek RC, Anthony TG. The eukaryotic initiation factor 2 kinase GCN2 protects against hepatotoxicity during asparaginase treatment. *American Journal of Physiology-Endocrinology and Metabolism*. 2013;305:E1124–E1133.

31. Phillipson-Weiner L, Mirek ET, Wang Y, McAuliffe WG, Wek RC, Anthony TG. General control nonderepressible 2 deletion predisposes to asparaginase-associated pancreatitis in mice. *American Journal of Physiology-Gastrointestinal and Liver Physiology*. 2016;310:G1061–G1070.

32. Obeid M, Tesniere A, Ghiringhelli F, Fimia GM, Apetoh L, Perfettini J-L, Castedo M, Mignot G, Panaretakis T, Casares N, Métivier D, Larochette N, van Endert P, Ciccosanti F, Piacentini M, Zitvogel L, Kroemer G. Calreticulin exposure dictates the immunogenicity of cancer cell death. *Nat Med*. 2007;13:54–61.

33. Apetoh L, Ghiringhelli F, Tesniere A, Obeid M, Ortiz C, Criollo A, Mignot G, Maiuri MC, Ullrich E, Saulnier P, Yang H, Amigorena S, Ryffel B, Barrat FJ, Saftig P, Levi F, Lidereau R, Nogues C, Mira J-P, Chompret A, Joulin V, Clavel-Chapelon F, Bourhis J, André F, Delaloge S, Tursz T, Kroemer G, Zitvogel L. Toll-like receptor 4–dependent contribution of the immune system to anticancer chemotherapy and radiotherapy. *Nat Med*. 2007;13:1050–1059.

34. Ravishankar B, Liu H, Shinde R, Chaudhary K, Xiao W, Bradley J, Koritzinsky M, Madaio MP, McGaha TL. The amino acid sensor GCN2 inhibits inflammatory responses to apoptotic cells promoting tolerance and suppressing systemic autoimmunity. *Proc Natl Acad Sci USA*. 2015;112:10774–10779.

35. Krysko DV, Kaczmarek A, Krysko O, Heyndrickx L, Woznicki J, Bogaert P, Cauwels A, Takahashi N, Magez S, Bachert C, Vandenabeele P. TLR-2 and TLR-9 are sensors of apoptosis in a mouse model of doxorubicin-induced acute inflammation. *Cell Death Differ*. 2011;18:1316–1325.

36. Pruenster M, Kurz ARM, Chung K-J, Cao-Ehlker X, Bieber S, Nussbaum CF, Bierschenk S, Eggersmann TK, Rohwedder I, Heinig K, Immler R, Moser M, Koedel U, Gran S, McEver RP, Vestweber D, Verschoor A, Leanderson T, Chavakis T, Roth J, Vogl T, Sperandio M. Extracellular MRP8/14 is a regulator of β2 integrin-dependent neutrophil slow rolling and adhesion. *Nat Commun*. 2015;6:6915.

37. Vogl T, Ludwig S, Goebeler M, Strey A, Thorey IS, Reichelt R, Foell D, Gerke V, Manitz MP, Nacken W, Werner S, Sorg C, Roth J. MRP8 and MRP14 control microtubule reorganization during transendothelial migration of phagocytes. *Blood*. 2004;104:4260–4268.

38. Ryckman C, Vandal K, Rouleau P, Talbot M, Tessier PA. Proinflammatory Activities of S100: Proteins S100A8, S100A9, and S100A8/A9 Induce Neutrophil Chemotaxis and Adhesion. *J Immunol*. 2003;170:3233–3242.

39. Christoffersson G, Vågesjö E, Vandooren J, Lidén M, Massena S, Reinert RB, Brissova M, Powers AC, Opdenakker G, Phillipson M. VEGF-A recruits a proangiogenic MMP-9–delivering neutrophil subset that induces angiogenesis in transplanted hypoxic tissue. *Blood*. 2012;120:4653–4662.

40. Soehnlein O, Zernecke A, Eriksson EE, Rothfuchs AG, Pham CT, Herwald H, Bidzhekov K, Rottenberg ME, Weber C, Lindbom L. Neutrophil secretion products pave the way for inflammatory monocytes. *Blood*. 2008;112:1461–1471.

41. Wang X, Abraham S, McKenzie JAG, Jeffs N, Swire M, Tripathi VB, Luhmann UFO, Lange CAK, Zhai Z, Arthur HM, Bainbridge J, Moss SE, Greenwood J. LRG1 promotes angiogenesis by modulating endothelial TGF-β signalling. *Nature*. 2013;499:306–311.

42. Singhal M, Gengenbacher N, Abdul Pari AA, Kamiyama M, Hai L, Kuhn BJ, Kallenberg DM, Kulkarni SR, Camilli C, Preuß SF, Leuchs B, Mogler C, Espinet E, Besemfelder E, Heide D, Heikenwalder M, Sprick MR, Trumpp A, Krijgsveld J, Schlesner M, Hu J, Moss SE, Greenwood J, Augustin HG. Temporal multi-omics identifies LRG1 as a vascular niche instructor of metastasis. *Sci Transl Med*. 2021;13:eabe6805.

43. Camilli C, Hoeh AE, De Rossi G, Moss SE, Greenwood J. LRG1: an emerging player in disease pathogenesis. *J Biomed Sci*. 2022;29:6.

44. Perros F, Günther S, Ranchoux B, Godinas L, Antigny F, Chaumais M-C, Dorfmüller P, Hautefort A, Raymond N, Savale L, Jaïs X, Girerd B, Cottin V, Sitbon O, Simonneau G, Humbert M, Montani D. Mitomycin-Induced Pulmonary Veno-Occlusive Disease: Evidence From Human Disease and Animal Models. *Circulation*. 2015;132:834–847.

45. Chen Z, Zhang J, Wei D, Chen J, Yang J. GCN2 Regulates ATF3-p38 MAPK Signaling Transduction in Pulmonary Veno-Occlusive Disease. *J Cardiovasc Pharmacol Ther*. 2021;26:677–689.

46. Santos-Ribeiro D, Lecocq M, De Beukelaer M, Verleden S, Bouzin C, Ambroise J, Dorfmuller P, Yakoub Y, Huaux F, Quarck R, Karmouty-Quintana H, Ghigna M-R, Bignard J, Nadaud S, Soubrier F, Horman S, Perros F, Godinas L, Pilette C. Disruption of GCN2 Pathway Aggravates Vascular and Parenchymal Remodeling During Pulmonary Fibrosis. *Am J Respir Cell Mol Biol*. 2022;

47. Lawrence MB, Springer TA. Neutrophils roll on E-selectin. *J Immunol*. 1993;151:6338–6346.

48. Meizlish ML, Franklin RA, Zhou X, Medzhitov R. Tissue Homeostasis and Inflammation. *Annu Rev Immunol*. 2021;39:557–581.

FIGURES LEGENDS

Figure 1. The integrated stress response is induced in WT rat lungs after systemic asparaginase exposure. (A) Bodyweight loss three days after a single injection of either asparaginase (ASNase; 75 units per kilogram body weight) or physiological serum in both WT rats (WT) and *Gcn2* KO rats (*Gcn2*$^{-/-}$). n^{male}=4 and $n^{femelle}$=4 per condition. (B) Pulmonary levels of phospho-GCN2 protein (general control nonderepressible 2; B1), GCN2 (B2), PERK [(PKR)-like endoplasmic reticulum kinase; B3] and ASNS (asparagine synthetase; B4) were analyzed by Western blotting in control and asparaginase-treated rats of both WT and *Gcn2*$^{-/-}$ genotypes. (C) Pulmonary levels of ATF4 (activating transcription factor 4; C1) and Sestrin-2 (C2) were analyzed by Western blotting in control and asparaginase-treated rats of both WT and *Gcn2*$^{-/-}$ genotypes. β-Actin was used as the loading control. *p<0.05, **p<0.005, ***p<0.0005 by two-way ANOVA test, except for B2: Mann-Whitney U test. n^{male}=3 and $n^{femelle}$=3 for rats treated with ASNase, n^{male}=3 and $n^{femelle}$=2 for rats treated with Vhcl.

Figure 2. Deficient autophagy and increased apoptosis in lungs from asparaginase-treated Gcn2-deficient rats. (A) Pulmonary levels of p62 (A1), ATG3 (A2), and LC3B (A3) were analyzed by Western blotting in control and asparaginase-treated rats of both WT and *Gcn2*$^{-/-}$ genotypes. n^{male}=3 and $n^{femelle}$=3 for each condition exept for *Gcn2*$^{-/-}$ rats treated with Vhcl, n^{male}=3 and $n^{femelle}$=2. (B) Immunofluorescent TUNEL staining of rat lungs (green, apoptosis marker). Nikon Eclipse Ti, 20X; Scalebar: 50µM. To quantify pulmonary apoptosis, the ratio of $TUNEL^{+}$ cells per total ($DAPI^{+}$) cell number was calculated. Images for control and treatment groups in microscopy experiments were collected at the same time under the same conditions. n^{male}=4 and $n^{femelle}$=3 for each condition exept for WT rats treated with Vhcl, n^{male}=3 and $n^{femelle}$=3. *p<0.05, **p<0.005, ***p<0.0005 by two-way ANOVA test.

Figure 3. Transcriptional profiling of lungs three days after a single injection of either asparaginase or physiological serum in both wild-type rats (WT) or Gcn2 KO rats (Gcn2$^{-/-}$). (A) Differentially expressed genes that are significantly either up- or downregulated between all experimental groups. (B) Venn diagram shows the number of genes altered by asparaginase treatment, with 1221 genes categorized as unique to

ASNase-treated *Gcn2*$^{-/-}$ rats, 27 genes unique to ASNase-treated WT rats, and 15 genes common to both ASNase-treated genotypes. (C) Heatmap representation of upregulated genes in asparaginase-treated *Gcn2*$^{-/-}$ rats classified by the Hallmark_inflammatory response gene set in all experiment groups. (D) Hallmark geneset enrichment analysis of asparaginase-treated *Gcn2*$^{-/-}$ rats versus asparaginase-treated WT rats showing the most significantly upregulated pathways. n^{male}=4 and $n^{femelle}$=4 for each condition except for *Gcn2*$^{-/-}$ rats treated with ASNase, n^{male}=4 and $n^{femelle}$=3

Figure 4. Asparaginase treatment induces inflammation in Gcn2-deficient rats (Gcn2$^{-/-}$). (A) Gene expression of Il1β (B) Nfkb2, n^{male}=4 and $n^{femelle}$=3 for each condition (C) Nfkb2, (D) Myd88, n^{male}=4 and $n^{femelle}$=3 for each condition except for *Gcn2*$^{-/-}$ rats treated with Vhcl, n^{male}=3 and $n^{femelle}$=3 (E) Myd88, and (F) SELE, n^{male}=4 and $n^{femelle}$=3 for each condition except for *Gcn2*$^{-/-}$ rats treated with ASNase, n^{male}=3 and $n^{femelle}$=3, in rat lungs measured by RT-qPCR. Each mRNA from a single biological sample was measured in triplicate, normalized to 18S ribosomal RNA, and means of triplicate values are compared. Results were obtained by the comparative Ct method and are expressed as fold change with respect to the experimental control. (G) Calprotectin concentration in the serum measured by ELISA. n^{male}=3 and $n^{femelle}$=3 for each condition. *p<0.05, **p<0.005, ***p<0.0005, ****p<0.0001 by two-way ANOVA test.

Figure 5. scRNA-seq identifies different cellular landscapes in the lungs of Gcn2-deficient rats and WT rats with either asparaginase treatment or under basal conditions. (A) UMAP projection of 18,201 lung cells from 12 rats showing the formation of 19 clusters. (B) Dot plot displaying average expression of discriminative marker genes used to identify cell clusters in (A). Dot size corresponds to percentage of cells expressing a gene in the cluster (C). Bar chart highlighting the percentage of cells per sample within each cell type cluster (WT rats treated with asparaginase in blue, WT rats treated with physiological serum in yellow, *Gcn2*-deficient rats treated with asparaginase in grey, and *Gcn2*-deficient rats treated with physiological serum in orange).

Figure 6. scRNA-seq reveals unique DEGs in cell types of Gcn2$^{-/-}$ rats compared to WT rats. (A) Jitter plot displaying differential gene expression for each cell type of the UMAP projection according to genotype

(*Gcn2*$^{-/-}$ rats injected with vehicle vs WT rats injected with vehicle) or according to asparaginase treatment and genotype (*Gcn2*$^{-/-}$ rats treated with asparaginase vs WT rats treated with asparaginase). Each dot represents genes distributed according to the log (fold change) of a gene. Dots with FDR < 0.05 are in color. Grey dots were not significant. (B) Dot plot presenting differentially expressed genes across cell types enabling the identification of genes whose differential expression was specific to an experiment group and a particular cell type. Abbreviations for cell types are defined in figure 5.

Figure 7. Flow cytometry and immunofluorescence validate scRNA-seq cell type identities. (A) Flow cytometry analysis of pulmonary cells from *Gcn2*-deficient rats and WT rats under basal conditions confirmed (A1) the increased population of $CD3^+$ $LAG3^+$ cells in unstressed *Gcn2*-deficient rats. This analysis enabled us to confirm that the increase of $LAG3^+$ T cells occurs in both $CD4^+$ (A2) and $CD8^+$ (A3) T cells. n^{male}=3 and $n^{femelle}$=2 for each condition. (B) Immunofluorescent staining of rat lungs for Ki67 (proliferation marker; green) and CD3 (lymphocyte T cell marker; red). Nikon Eclipse Ti, 20X ; Scalebar : 50µM. To quantify proliferating CD3+ cells, the ratio of double-positive Ki67+ CD3+ cells over total cells was calculated. Images for control and treatment groups in microscopy experiments were collected at the same time under the same conditions. n^{male}=3 and $n^{femelle}$=2 for *Gcn2*$^{-/-}$ rats, n^{male}=2 and $n^{femelle}$=2 for WT rats. *p<0.05, **p<0.005, ***p<0.0005, ****p<0.0001 by two-way ANOVA test, except for (A1), (A2), and (A3): Mann Whitney U test.

Figure 8. Expression of innate immunity cell markers in rat lungs under ASnase treatment. (A) Immunofluorescent double-staining of rat lungs from the four groups using a human monoclonal antibody against CD11b and a goat antiserum again rat S100A8 subunit of calprotectin. Nikon Eclipse Ti, 20X ; Scalebar : 50µM. White arrows indicate staining by either antibody or both in the lung from the various conditions. (B) To quantify calprotectin+ cells, the ratio of CD11b + or calprotectin+ or double positive labelled cells over total (DAPI+) cells was calculated. Kruskall-Wallis, ANOVA 1 Way on log-transformed values. n^{male}=2 and $n^{femelle}$=2 for each condition except for *Gcn2*$^{-/-}$ rats treated with ASNase, n^{male}=4 and $n^{femelle}$=3. (C) Pulmonary levels of MMP9 were analyzed by Western blotting in control and asparaginase-

treated rats for both WT and *Gcn2*$^{-/-}$ genotypes. β-Actin was used as the loading control. n^{male}=3 and $n^{femelle}$=3 for each condition. Images for control and treatment groups in microscopy experiments were collected at the same time under the same conditions. *p<0.05, **p<0.005, ***p<0.0005, ****p<0.0001 by two-way ANOVA test.

Figure 9. Rat Luminex Assay. Luminex assay (R&D LXSARM-17) was performed according to the manufacturer procedure, with rat plasma from the four groups ; n^{male}=3 and $n^{femelle}$=3 for each condition *p<0.05, **p<0.005, ***p<0.0005

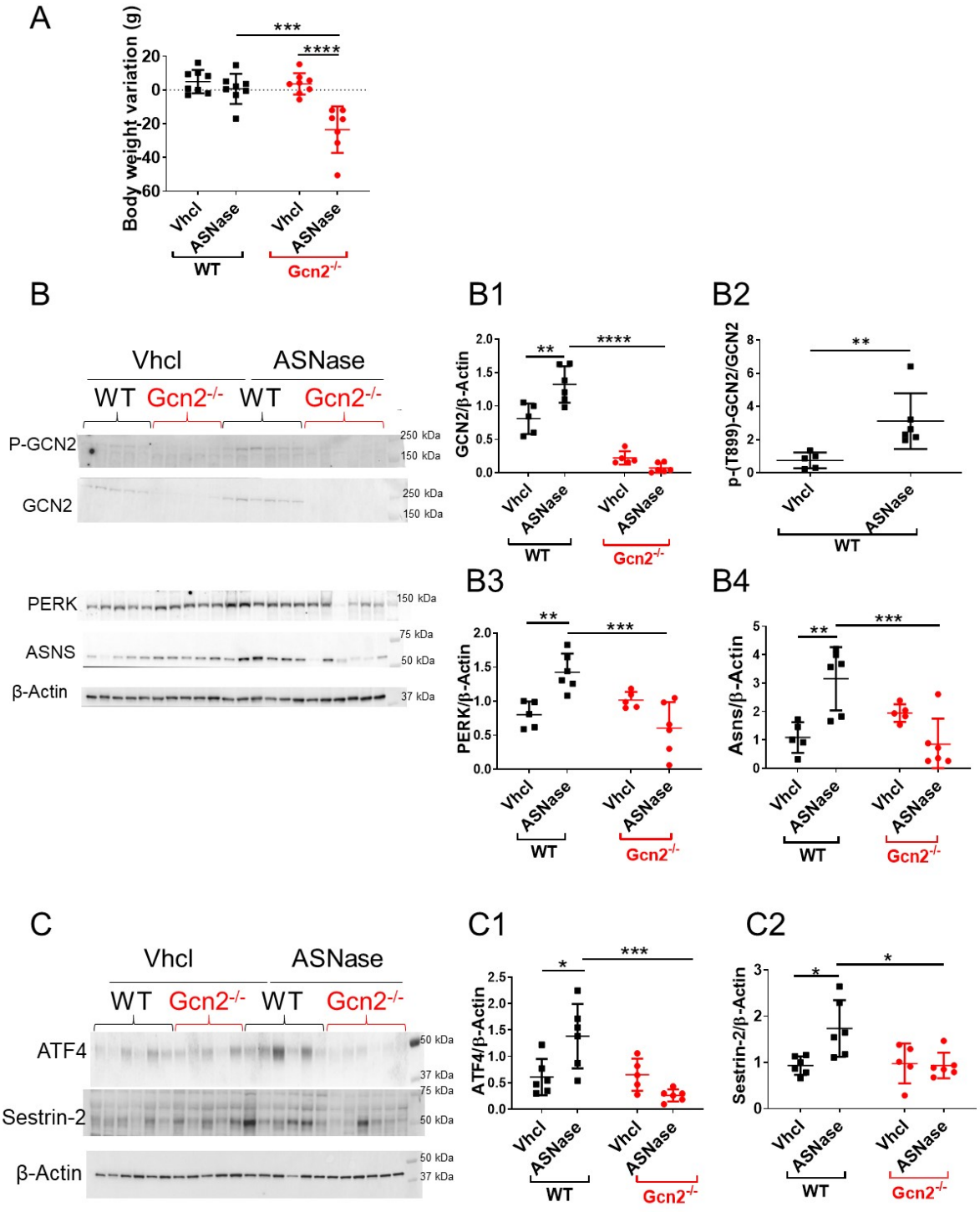
A
Body weight variation (g)
20
0
-20
-40
-60
***
****
Vhcl
ASNase
Vhcl
ASNase
WT
Gcn2-/-
B
Vhcl
ASNase
WT
Gcn2-/-
WT
Gcn2-/-
P-GCN2
250 kDa
150 kDa
GCN2
250 kDa
150 kDa
PERK
150 kDa
ASNS
75 kDa
50 kDa
β-Actin
37 kDa
B1
GCN2/β-Actin
2.0
1.5
1.0
0.5
0.0
**
****
Vhcl
ASNase
Vhcl
ASNase
WT
Gcn2-/-
B2
p-(T899)-GCN2/GCN2
8
6
4
2
0
**
Vhcl
ASNase
WT
B3
PERK/β-Actin
2.0
1.5
1.0
0.5
0.0
**
***
Vhcl
ASNase
Vhcl
ASNase
WT
Gcn2-/-
B4
Asns/β-Actin
5
4
3
2
1
0
**
***
Vhcl
ASNase
Vhcl
ASNase
WT
Gcn2-/-
C
Vhcl
ASNase
WT
Gcn2-/-
WT
Gcn2-/-
ATF4
50 kDa
37 kDa
Sestrin-2
75 kDa
50 kDa
β-Actin
50 kDa
37 kDa
C1
ATF4/β-Actin
2.5
2.0
1.5
1.0
0.5
0.0
*
***
Vhcl
ASNase
Vhcl
ASNase
WT
Gcn2-/-
C2
Sestrin-2/β-Actin
3
2
1
0
*
*
Vhcl
ASNase
Vhcl
ASNase
WT
Gcn2-/-

Figure 1

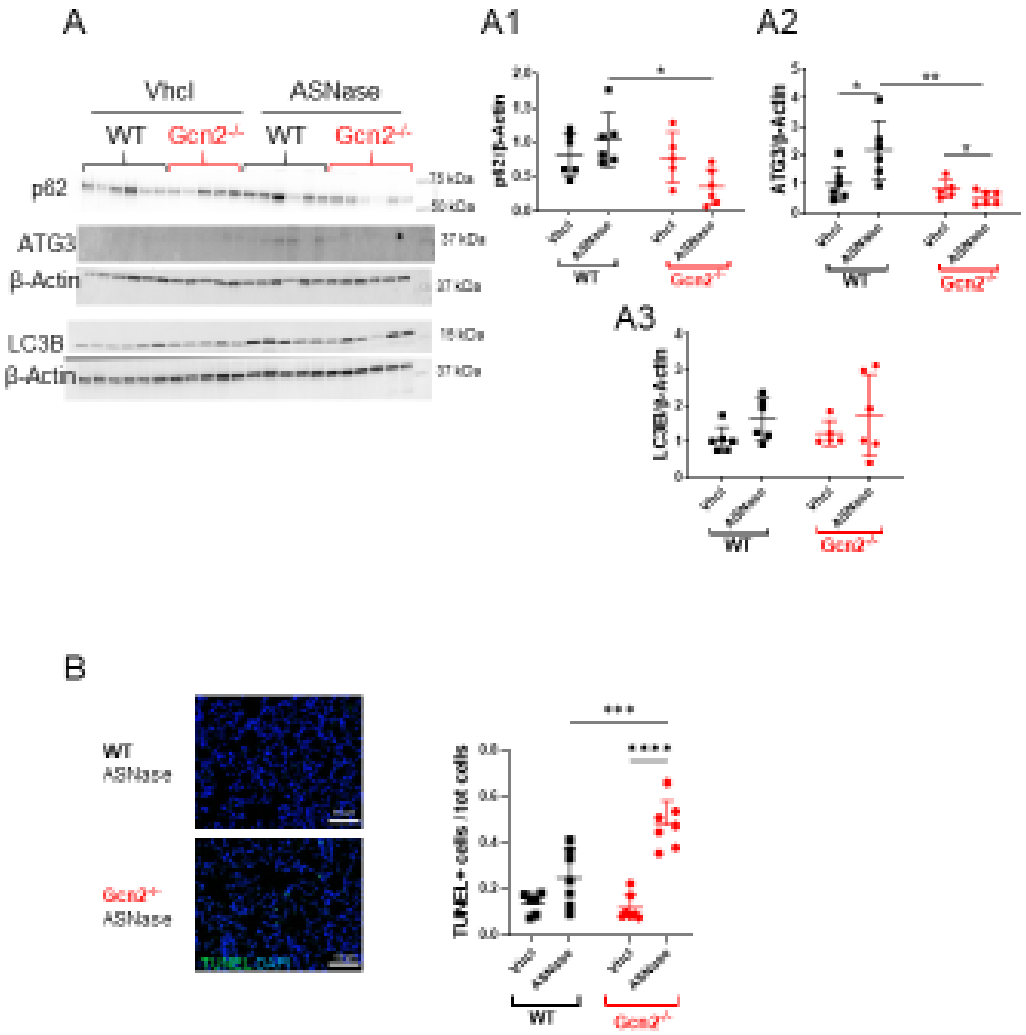
A
Vhcl
ASNase
WT
Gcn2-/-
WT
Gcn2-/-
p62
ATG3
β-Actin
LC3B
β-Actin
75 kDa
50 kDa
37 kDa
27 kDa
15 kDa
37 kDa
A1
p62/β-Actin
A2
ATG3/β-Actin
A3
LC3B/β-Actin
B
WT
ASNase
Gcn2-/-
ASNase
TUNEL+ cells / tot cells
***
****

Figure 2

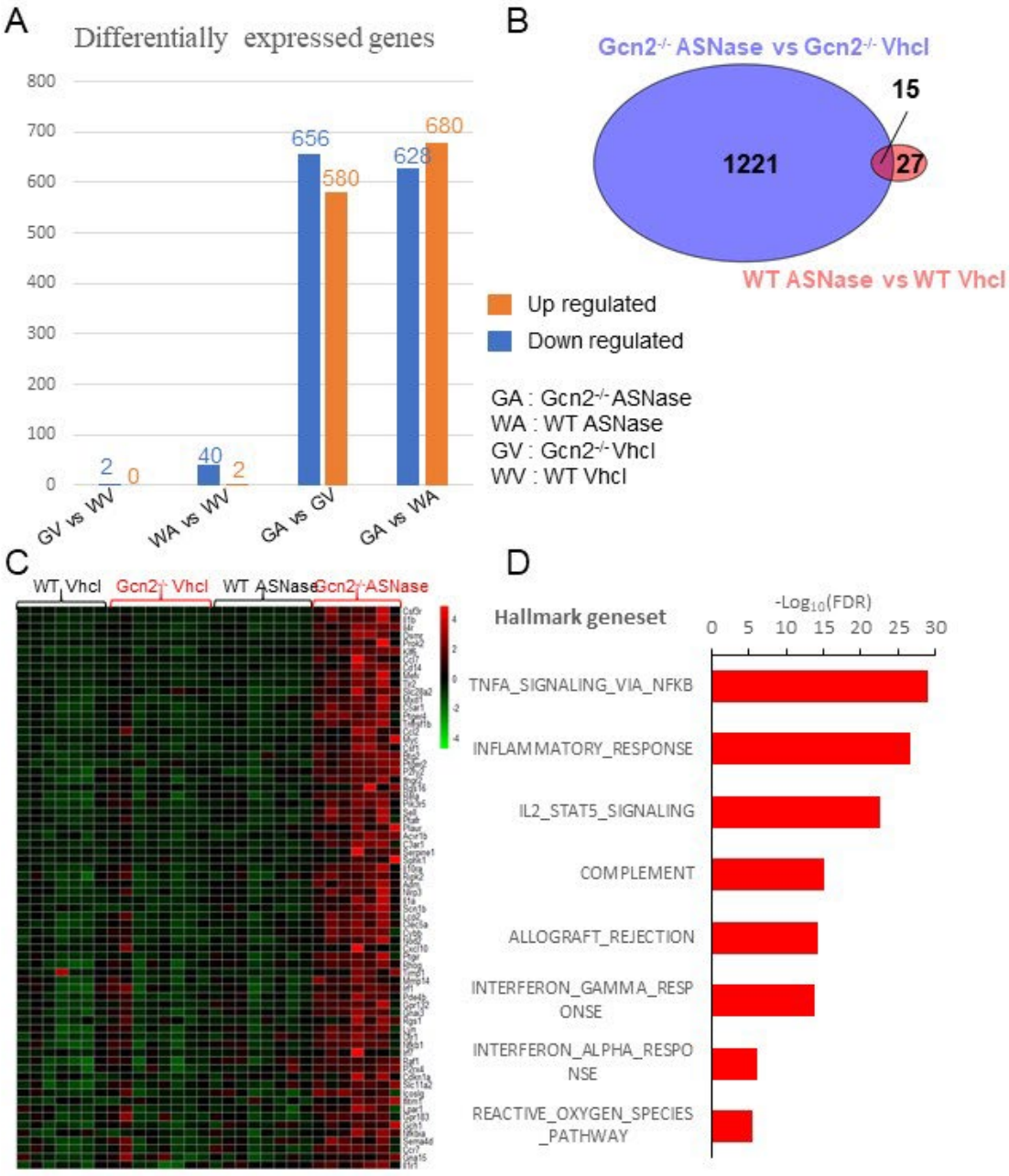
A
Differentially expressed genes
800
700
600
500
400
300
200
100
0
2
0
40
2
656
580
628
680
GV vs WV
WA vs WV
GA vs GV
GA vs WA
Up regulated
Down regulated
GA : Gcn2-/- ASNase
WA : WT ASNase
GV : Gcn2-/- Vhcl
WV : WT Vhcl
B
Gcn2-/- ASNase vs Gcn2-/- Vhcl
1221
15
27
WT ASNase vs WT Vhcl
C
WT Vhcl
Gcn2-/- Vhcl
WT ASNase
Gcn2-/- ASNase
D
Hallmark geneset
-Log10(FDR)
0 5 10 15 20 25 30
TNFA_SIGNALING_VIA_NFKB
INFLAMMATORY_RESPONSE
IL2_STAT5_SIGNALING
COMPLEMENT
ALLOGRAFT_REJECTION
INTERFERON_GAMMA_RESPONSE
INTERFERON_ALPHA_RESPONSE
REACTIVE_OXYGEN_SPECIES_PATHWAY

Figure 3

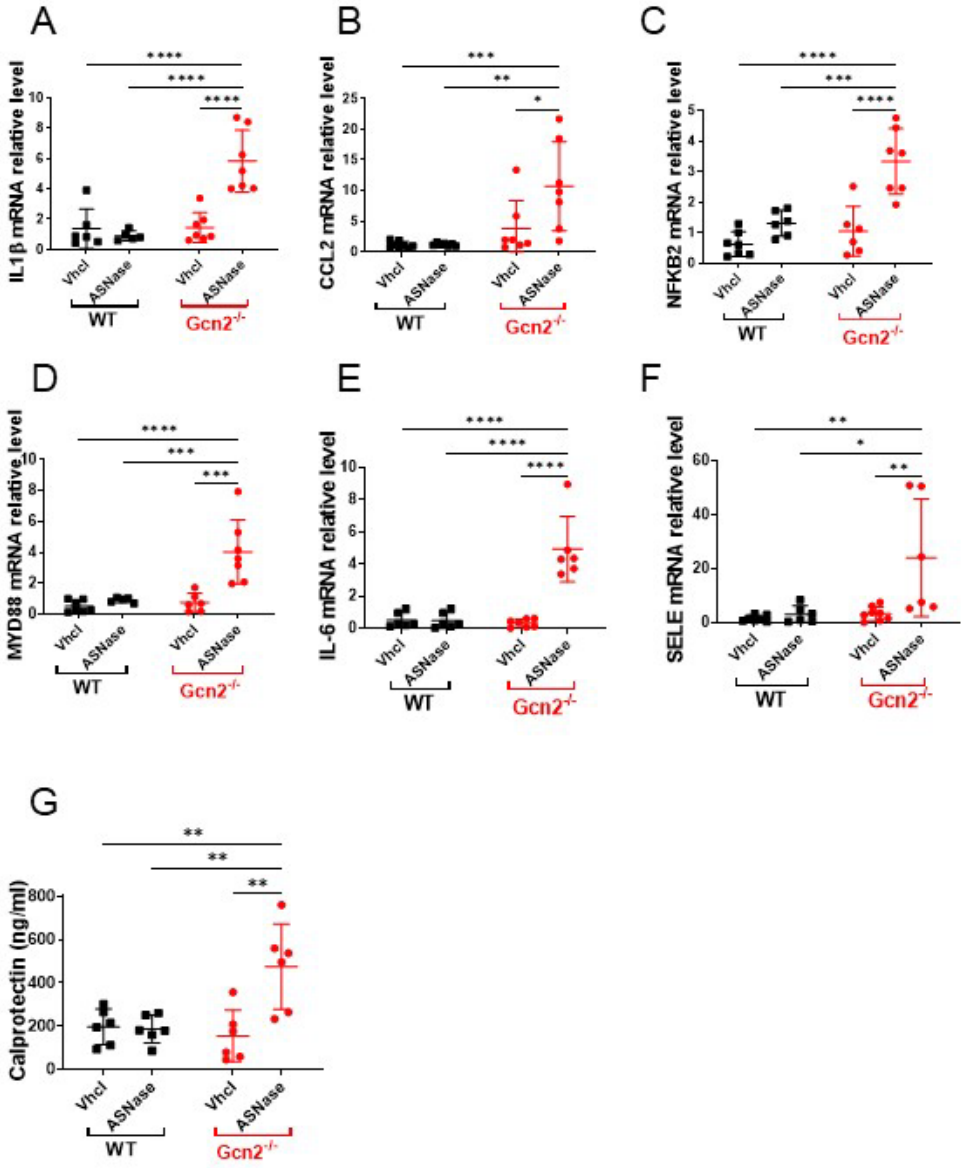
A
IL1β mRNA relative level
B
CCL2 mRNA relative level
C
NFKB2 mRNA relative level
D
MYD88 mRNA relative level
E
IL-6 mRNA relative level
F
SELE mRNA relative level
G
Calprotectin (ng/ml)
Vhcl
ASNase
WT
Gcn2-/-

Figure 4

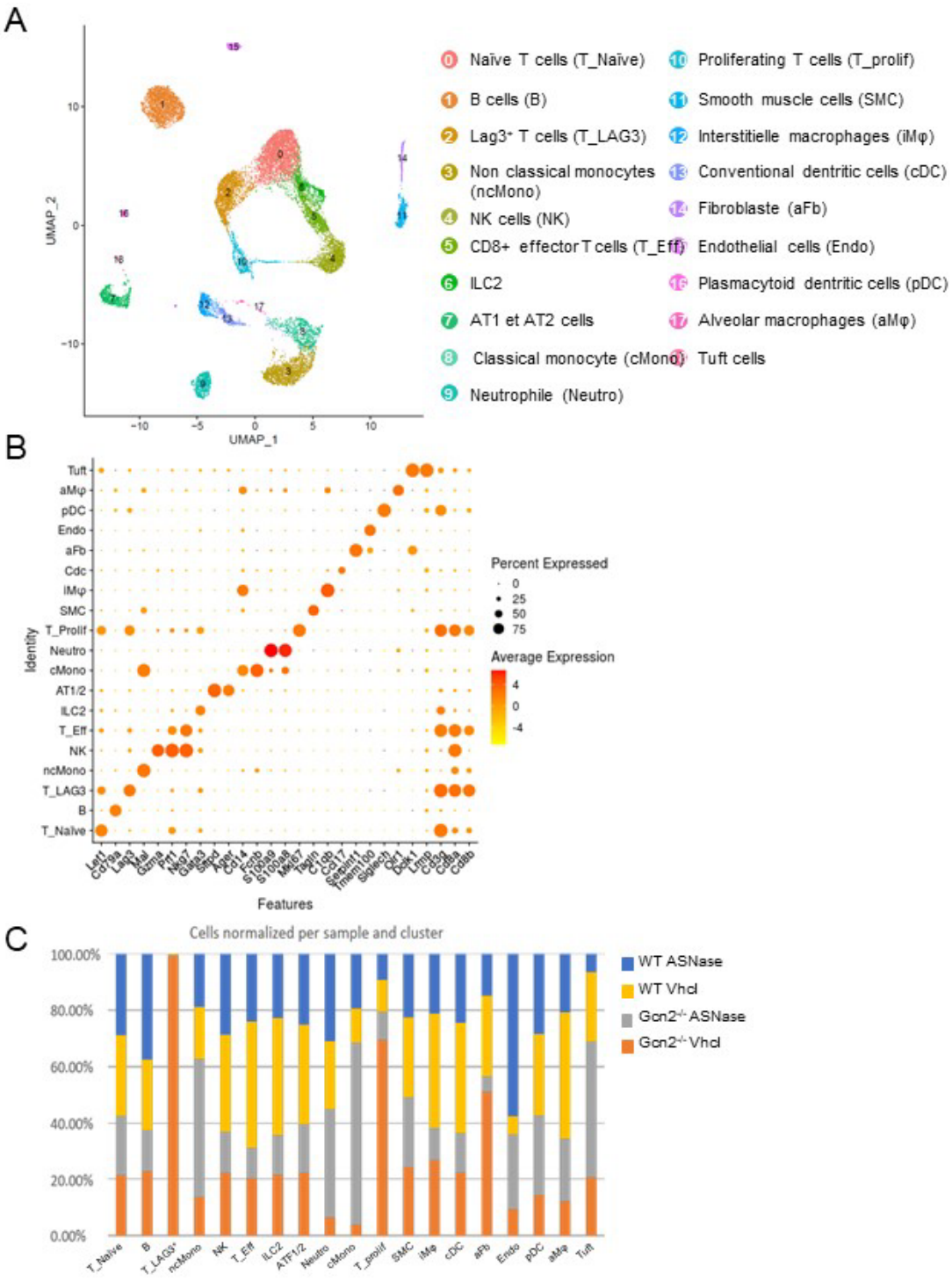
A
UMAP_1
UMAP_2
0 Naïve T cells (T_Naïve)
1 B cells (B)
2 Lag3+ T cells (T_LAG3)
3 Non classical monocytes (ncMono)
4 NK cells (NK)
5 CD8+ effector T cells (T_Eff)
6 ILC2
7 AT1 et AT2 cells
8 Classical monocyte (cMono)
9 Neutrophile (Neutro)
10 Proliferating T cells (T_prolif)
11 Smooth muscle cells (SMC)
12 Interstitielle macrophages (iMφ)
13 Conventional dentritic cells (cDC)
14 Fibroblaste (aFb)
15 Endothelial cells (Endo)
16 Plasmacytoid dentritic cells (pDC)
17 Alveolar macrophages (aMφ)
18 Tuft cells
B
Identity
Tuft
aMφ
pDC
Endo
aFb
Cdc
IMφ
SMC
T_Prolif
Neutro
cMono
AT1/2
ILC2
T_Eff
NK
ncMono
T_LAG3
B
T_Naïve
Features
Percent Expressed
0
25
50
75
Average Expression
4
0
-4
C
Cells normalized per sample and cluster
100.00%
80.00%
60.00%
40.00%
20.00%
0.00%
WT ASNase
WT Vhcl
Gcn2-/- ASNase
Gcn2-/- Vhcl
T_Naïve
B
T_LAG3+
ncMono
NK
T_Eff
ILC2
AT1/2
Neutro
cMono
T_prolif
SMC
iMφ
cDC
aFb
Endo
pDC
aMφ
Tuft

Figure 5

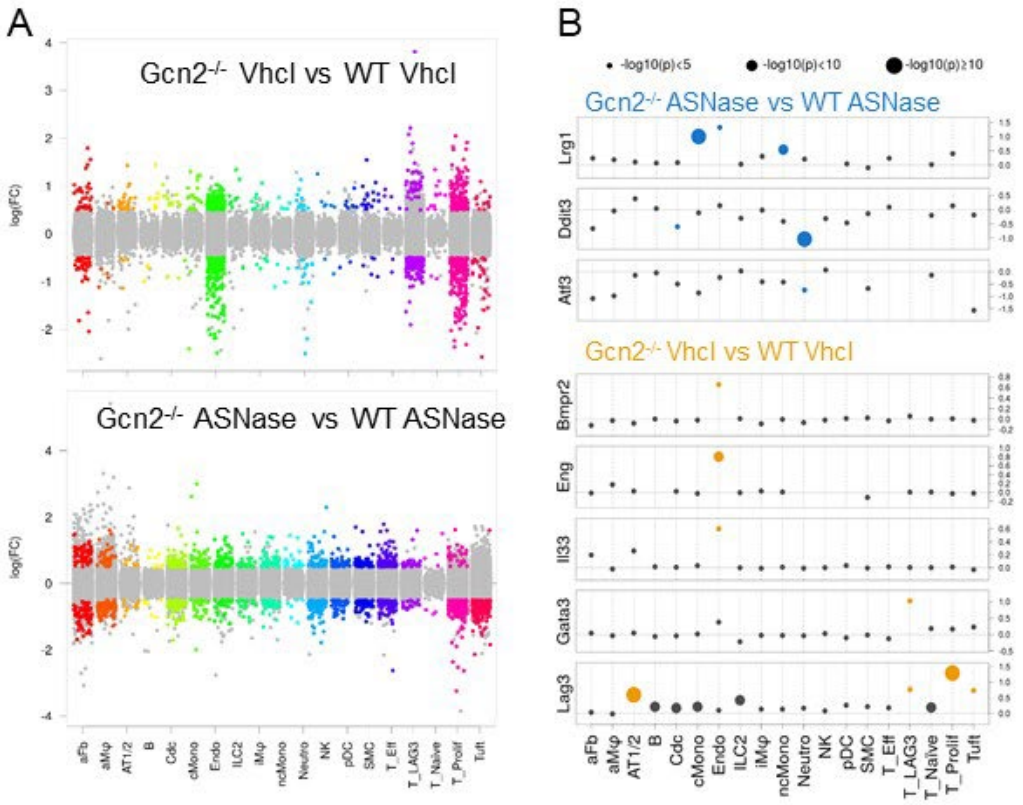
A
Gcn2-/- Vhcl vs WT Vhcl
Gcn2-/- ASNase vs WT ASNase
log(FC)
aFb
aMφ
AT1/2
B
Cdc
cMono
Endo
ILC2
iMφ
ncMono
Neutro
NK
pDC
SMC
T_Eff
T_LAG3
T_Naive
T_Prolif
Tuft
B
-log10(p)<5
-log10(p)<10
-log10(p)≥10
Gcn2-/- ASNase vs WT ASNase
Lrg1
Ddit3
Atf3
Gcn2-/- Vhcl vs WT Vhcl
Bmpr2
Eng
Il33
Gata3
Lag3

Figure 6

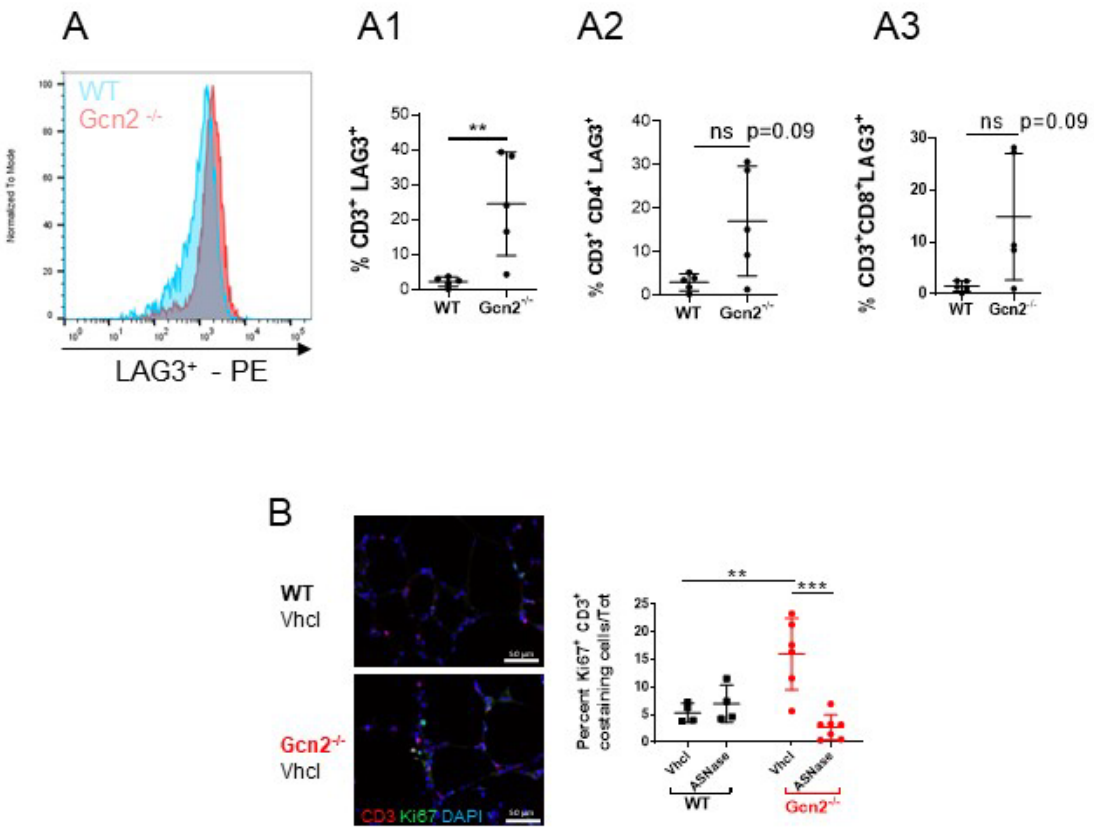
A
A1
A2
A3
WT
Gcn2 -/-
Normalized To Mode
LAG3+ - PE
% CD3+ LAG3+
**
WT
Gcn2-/-
% CD3+ CD4+ LAG3+
ns p=0.09
% CD3+CD8+LAG3+
B
WT
Vhcl
Gcn2-/-
Vhcl
CD3 Ki67 DAPI
Percent Ki67+ CD3+ costaining cells/Tot
***
Vhcl
ASNase

Figure 7

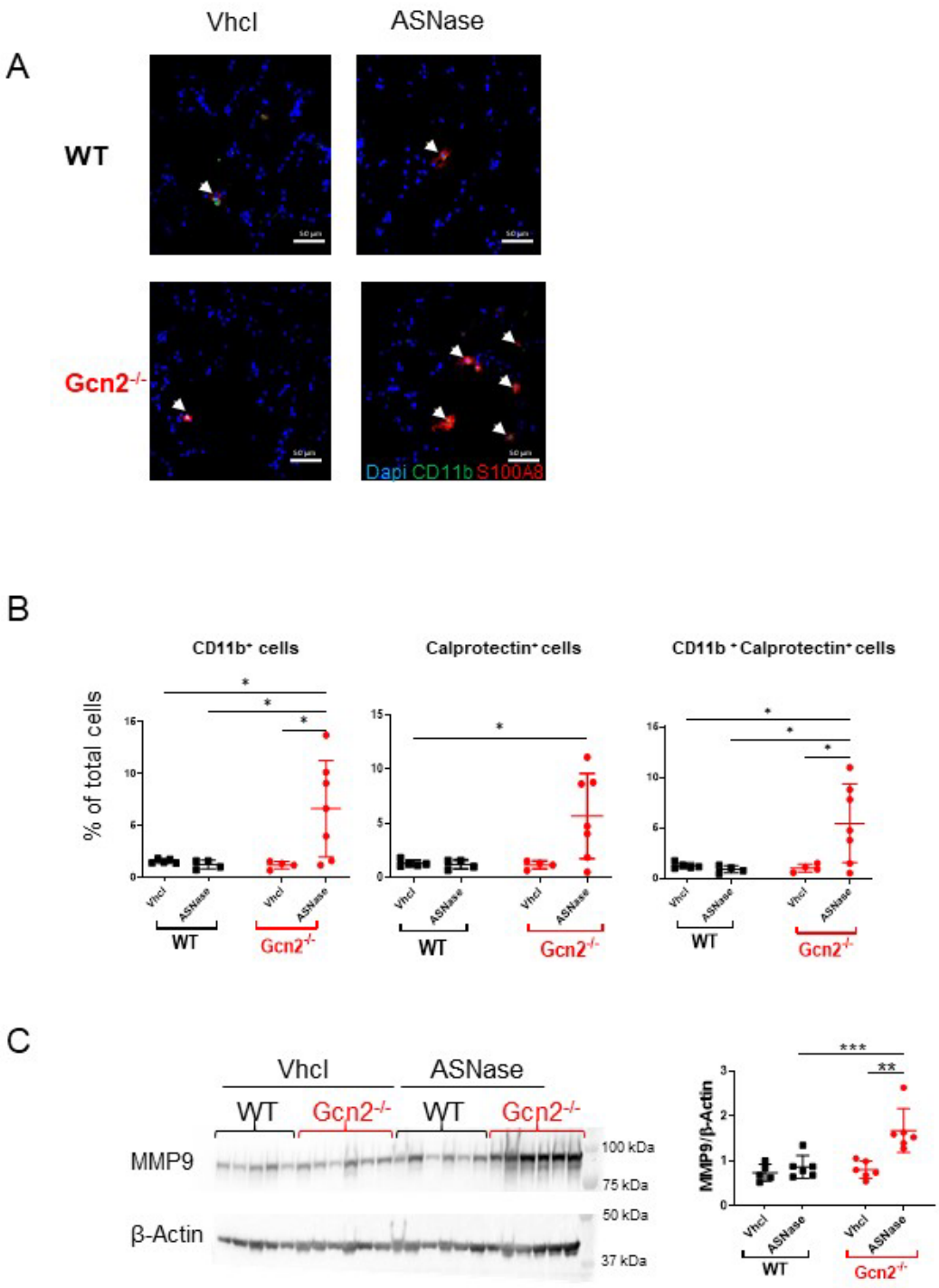
A
Vhcl
ASNase
WT
Gcn2-/-
Dapi CD11b S100A8
B
CD11b+ cells
Calprotectin+ cells
CD11b+Calprotectin+ cells
% of total cells
Vhcl
ASNase
WT
Gcn2-/-
C
Vhcl
ASNase
WT
Gcn2-/-
MMP9
β-Actin
100 kDa
75 kDa
50 kDa
37 kDa
MMP9/β-Actin

Figure 8